COMMUNICATIONS MATERIALS

ARTICLE

https://doi.org/10.1038/s43246-020-0031-4 OPEN

Simple and fast fabrication of single crystal VO_2 microtube arrays

Chunwang Zhao [1,2]✉, Shuxiang Ma[1,4], Zijian Li[3,4], Weiya Li[2], Jijun Li[2], Qingyu Hou[2] & Yongming Xing[2]✉

Single crystal VO_2 is a strongly correlated electron material that has shown great potential for a wide range of high-performance modern device applications, such as microbolometers, lithium ion batteries, microactuators and strain sensors. However, the present fabrication methods for single crystal VO_2 almost always require complicated procedures, strict conditions and long reaction times of up to one week. Here, we report a simple, fast, low-cost and green method for fabricating single crystal VO_2 using a thermal oxidation route based on resistive heating of a vanadium foil in air. Our method not only reduces the complete fabrication time from hours to tens of seconds but also naturally forms single crystal VO_2 microtube arrays that are nearly vertically aligned on the surface of a V_2O_5 substrate. Microstructure characteristics and the reversible phase transition between the monoclinic VO_2 and rutile VO_2 phases demonstrate that the obtained single crystal VO_2 is the same as that achieved by other fabrication methods.

[1] College of Arts and Sciences, Shanghai Maritime University, Shanghai 201306, China. [2] College of Science, Inner Mongolia University of Technology, Hohhot 010051, China. [3] Merchant Marine College, Shanghai Maritime University, Shanghai 201306, China. [4] These authors contributed equally: Shuxiang Ma, Zijian Li. ✉email: cwzhao@shmtu.edu.cn; xym@imut.edu.cn

Vanadium dioxide (VO_2) is an archetypal metal-insulator transition (MIT) material, which has received increasing attention in the exploration of the MIT mechanism[1–3] and has applications in various modern devices, such as electronic inks[4], supercapacitors[5], thermal diodes[6], thermal emitters[7], smart windows[8], temperature sensors[9], and radiative thermal memristors[10]. The MIT of VO_2 features a dramatic change in the electrical conductivity, optical reflectivity, magnetic susceptibility, and dielectric function because of the accompanying reversible structural phase transition between the monoclinic insulating phase (M1) and the tetragonal metallic phase (rutile structure, R) at approximately 67 °C[11]. The phase transition characteristics and the physical properties of VO_2 are strongly related to its stoichiometry, crystallinity, and morphology, which are generally determined by the fabrication methods[12]. Representative fabrication methods include reactive sputtering[1], pulsed laser deposition[2,3,6], hydrothermal methods[4], electrodeposition[5], molecular beam epitaxy[8], chemical vapor deposition[13], thermolysis[14], and magnetron sputtering[15] for polycrystalline VO_2 films or nanoparticles. Despite the potential large-scale applications of polycrystalline VO_2, the poor crystal quality and weak MIT properties[12] make it difficult for polycrystalline VO_2 to meet the requirements of high-performance modern devices.

In contrast, single crystal VO_2 has excellent MIT properties[11,12], which not only has been utilized for exploring intrinsic MIT physics[16,17] but also has demonstrated great potential for manufacturing high-performance microbolometers[18], lithium-ion batteries[19], microactuators[20], and highly sensitive strain sensors[21]. So far, various methods have been utilized for fabricating single crystal VO_2[11,12]. Several representative fabrication methods such as self-flux method, solution growth technique, vapor transport method, and hydrothermal method are briefly introduced as follows. The self-flux method[16,22] can fabricate high-quality single crystal VO_2 microrods with lengths of a few millimeters and widths of ~100 μm by heating V_2O_5 powder to 800–1100 °C in a vacuum tube furnace. During heating, the V_2O_5 is partially reduced and converts to single crystal VO_2 in the molten V_2O_5. However, the fabrication time is very long and is approximately 1 week[23]. The solution growth technique[24,25] can fabricate bulk single crystal VO_2 with lengths of up to greater than 10 mm and widths of up to 1 mm by heating a mixture of VO_2 powder and V_2O_5 powder, which are sealed in a silica tube up to 1050 °C and slowly cooled up to 100 h to 775 °C[25]. The rod-like bulk single crystal VO_2 grows along the high-temperature rutile c axis during heating and cooling process[24]. The vapor transport method[17,18,20] can fabricate rectangular cross-sectional single crystal VO_2 nanowires with lengths of tens of micrometers and widths of tens of nanometers to a few micrometers by evaporating V_2O_5[17,18,20] powder or VO_2[26] powder at approximately 950 °C and transporting the vapor by Ar carrier gas to a substrate in a quartz tube furnace. Although the fabrication time of the vapor transport method is much shorter than that of the self-flux method or solution growth technique, the fabrication time is still too long, approximately 5 h[26]. Recently, it was reported that the hydrothermal method can also be utilized to fabricate nearly round cross-sectional single crystal VO_2 nanowires with lengths of tens of micrometers and widths of hundreds of nanometers by heating an aqueous solution of V_2O_5, $H_2C_2O_4{\cdot}2H_2O$, and H_2SO_4 at 100 °C for 10 h, followed by heating the as-obtained precursor solution at 260 °C for 24 h[27]. This method realized massively production of single crystal VO_2 nanowires. However, the fabrication time is also very long. To date, high-quality single crystal VO_2 with different sizes from nanometers to millimeters can be fabricated as reviewed above; however, fabricating single crystal VO_2 via these present methods not only requires complicated procedures[17–19,21,24,25,27], strict conditions[17–19,21,24–27], or special equipment[16–18,21,22,24–26], but also consumes a great deal of energy because of the very long heating times; thus, these methods are costly.

In this work, we report a simple method for fabricating single crystal VO_2 via a thermal oxidation route[28] based on the resistive heating[29] of V foils in air using an ordinary laboratory power supply. The complete fabrication time is only tens of seconds, which is the fastest method for fabricating single crystal VO_2 to date. Interestingly, the as-fabricated single crystal VO_2 with a length of up to 430 μm and an average width of approximately 6.8 μm naturally forms high-density microtube arrays that are nearly vertically aligned on the surface of a V_2O_5 substrate without additional treatments. Moreover, the only required raw materials are commercially pure V foil and air, the as-fabricated products are only VO_2 and V_2O_5, and there is no waste; thus, our fabrication method has a low cost and is environmentally friendly.

Results

Fabrication of single crystal VO_2 microtube arrays. The fabrication of single crystal VO_2 microtube arrays contains two successive processes, i.e., heating a V foil in air with a direct current to approximately 1700 °C in tens of seconds to synthesize vanadium oxide on the surface of the V foil and then cooling the as-synthesized vanadium oxide to below 250 °C in a few seconds (Supplementary Movie 1). Figure 1 depicts a typical temperature vs. time curve for the growth process of single crystal VO_2 microtube arrays. Here, each temperature recorded by a pyrometer (temperature range of 250–2000 °C) refers to the temperature of the central region of the V foil, i.e., the highest temperature throughout the V foil. At the beginning of the heating process, the surface of the V foil is oxidized gradually in air (photograph no. 1, inset in Fig. 1), and the as-synthesized product is a mixture of solid vanadium oxide (VO_x, where x is the O–V atomic ratio), mainly V_2O_5 and VO_2[29], when the temperature of the V foil is below 678 °C (the melting point of bulk V_2O_5[30]). With continuous heating, the temperature of the V foil and as-synthesized solid VO_x continually increases to over 678 °C. The solid VO_x melts into a liquid and gradually forms two droplets[31] that cover both sides of the V foil (photograph no. 2, inset in Fig. 1). Obviously, the liquid droplets increase in thickness as the temperature continually increases, which means that additional VO_x is synthesized. When the temperature of the V foil as well as the VO_x liquid droplets further increases to approximately 1700 °C by continuous heating, the V foil reaches an incandescent state (photograph no. 3, inset in Fig. 1). At this point, the V atoms can largely dissociate from the V foil and diffuse into the VO_x liquid droplets, which makes the V content and the thickness of the liquid droplets increase largely.

Next, after the heating is stopped by turning off the direct current manually, the temperature of the VO_x liquid droplets decreases from ~1700 °C to below 250 °C at a very rapid rate of approximately 370 °C/s because of the natural heat dissipation. During cooling, it is found that the liquid droplets experience two crystallization processes in sequence that correspond to the platform and the trough in the temperature vs. time curve (marked with two rectangles in Fig. 1). When the temperature drops to approximately 833 °C, a large number of single crystal VO_2 microtubes grow in the liquid droplets and form arrays that stand in the residual liquid VO_x in less than 1 s (photograph no. 4, inset in Fig. 1). This crystallization process is exothermic, which maintains the crystallization starting temperature of VO_2 for a short time. As a result, a platform at ~833 °C appears in the temperature vs. time curve, as shown in the navy box inset in Fig. 1. After the VO_2 crystallization finishes, the whole product

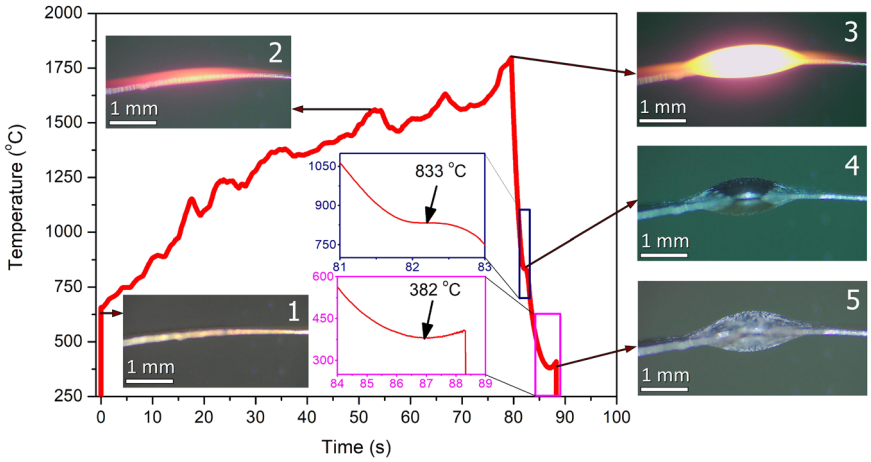

Fig. 1 Growth process of single crystal VO_2 microtube arrays. The curve depicts the change of temperature with time during the growth process. Insets no. 1–5 show the photographs of the V foil and the as-synthesized products at corresponding temperatures. At the beginning of heating (0 s), the temperature jumps to above 500 °C from room temperature at a very rapid and uncontrolled rate when turning on the direct current because of the very low resistance of the V foil, which results in a very large direct current being suddenly applied to the V foil.

resumes rapid cooling to approximately 382 °C. The residual liquid VO_x crystallizes and finally forms a solid V_2O_5 substrate with the as-crystallized single crystal VO_2 microtube arrays nearly vertically aligned on the surface of it (photograph no. 5, inset in Fig. 1). This crystallization process is also exothermic, which can even increase the temperature by up to 27 °C compared with the crystallization equilibrium temperature of V_2O_5 (382 °C) in more than 1 s. As a result, a trough at ~382 °C appears in the temperature vs. time curve, as shown in the magenta box inset in Fig. 1. After the V_2O_5 crystallization finishes, the whole product resumes rapid cooling again until it reaches room temperature.

To find the key fabrication conditions for single crystal VO_2 microtube arrays, we carried out many fabrication runs with different fabrication parameters. Supplementary Fig. 1 depicts the temperature vs. time curves of 14 successful fabrication runs for single crystal VO_2 microtube arrays using 14 V foils with different heating rates, cooling rates, peak temperatures, fabrication times, and crystallization temperatures, as summarized in Supplementary Table 1. We found that these fabrication parameters have wide ranges. The heating rate can occur over a range from 18 to 46 °C/s with an average of 28 °C/s, the peak temperature can occur over a range from 1613 to 1955 °C with an average of 1782 °C, and the fabrication time can occur over a range from 44 to 99 s with an average of 73 s; all can be easily controlled by adjusting the direct current manually. Moreover, the cooling rates range from 312 to 677 °C/s, with an average of 442 °C/s, without being controlled. The crystallization temperatures of VO_2 and V_2O_5 can occur over a range from 813 to 834 °C with an average of 824 °C and from 317 to 398 °C with an average of 353 °C, respectively. Additionally, we also carried out two unsuccessful fabrication runs with the following fabrication parameters. (1) The as-synthesized VO_x liquid droplets are rapidly cooled to below 250 °C (with a cooling rate of ~345 °C/s, shown by the red curve in Supplementary Fig. 2a) after gradually heating the V foil to a relatively low temperature of 1005 °C. It is found that irregular bumps are produced on the surface of the V foil, and there are no microtube arrays, as shown in Supplementary Fig. 2b. X-ray diffraction (XRD) examination demonstrated that the obtained product is mainly V_2O_5 with small amounts of VO_2 (the red curve in Supplementary Fig. 2d). An explanation is presented as Supplementary Note 1. (2) The as-synthesized VO_x liquid droplets are slowly cooled to below 250 °C (with a cooling rate of ~29 °C/s, as shown by the blue curve in Supplementary Fig. 2a) after gradually heating the V foil to a high temperature of 1785 °C. Only plate-shaped solids are produced on the surface of V foil, and there are no microtube arrays, as shown in Supplementary Fig. 2c. XRD examination demonstrated that the obtained product is a pure phase of V_2O_5 (blue curve in Supplementary Fig. 2d). An explanation is presented as Supplementary Note 2. Consequently, we propose that the V foil must be gradually heated to incandescent temperature and then rapidly cooled to fabricate single crystal VO_2 microtube arrays.

Characterization of single crystal VO_2 microtube arrays. The morphology, composition, and microstructure of the as-fabricated product were examined using scanning electron microscopy (SEM), X-ray energy dispersive spectroscopy (EDS), X-ray photoelectron spectroscopy (XPS), XRD, and transmission electron microscopy (TEM). As shown in the representative SEM images in Fig. 2a (side view), Fig. 2b (top view), and in the lower-left inset in Fig. 2a, single crystal VO_2 are straight, rod-like and nearly vertically aligned on the surface of a layered V_2O_5 substrate (Supplementary Fig. 3). The upper-right inset in Fig. 2a and the upper-right inset in Fig. 2b show that these single crystal VO_2 microtubes are all hollow and have rectangular cross-sections and steeple-shaped tops. It is also noticed that there are small amounts of solidified V_2O_5 flux on the side surface of the VO_2 microtubes[25], which are further observed by high-resolution TEM (HRTEM) and analyzed below. The EDS mapping of an individual microtube confirms that only V and O are present and uniformly distributed over the whole microtube, as shown in the lower-right inset of Fig. 2b. Additional EDS spectrums (Supplementary Fig. 4) demonstrate that the O–V atomic ratio are ~1.98 and ~2.49 for the VO_2 microtube and the V_2O_5 substrate, respectively. The widths of different microtubes vary from 1 to 12 μm (Fig. 2c) with an average width of ~6.8 μm, while each microtube has a uniform width along its entire length. The length of those microtubes can reach up to 430 μm. Obviously, the density (~450 mm^{-2}) of the VO_2 microtube arrays is very high and reaches that of ultra-dense (400–2000 mm^{-2}) VO_2 nanowires fabricated by the vapor transport method[32]. To the best of our knowledge, this special morphology of our single crystal VO_2 microtube arrays has never been reported before for single crystal or polycrystalline VO_2[11,12]. Moreover, the as-fabricated product was characterized by XPS. As shown in Supplementary Fig. 5, the

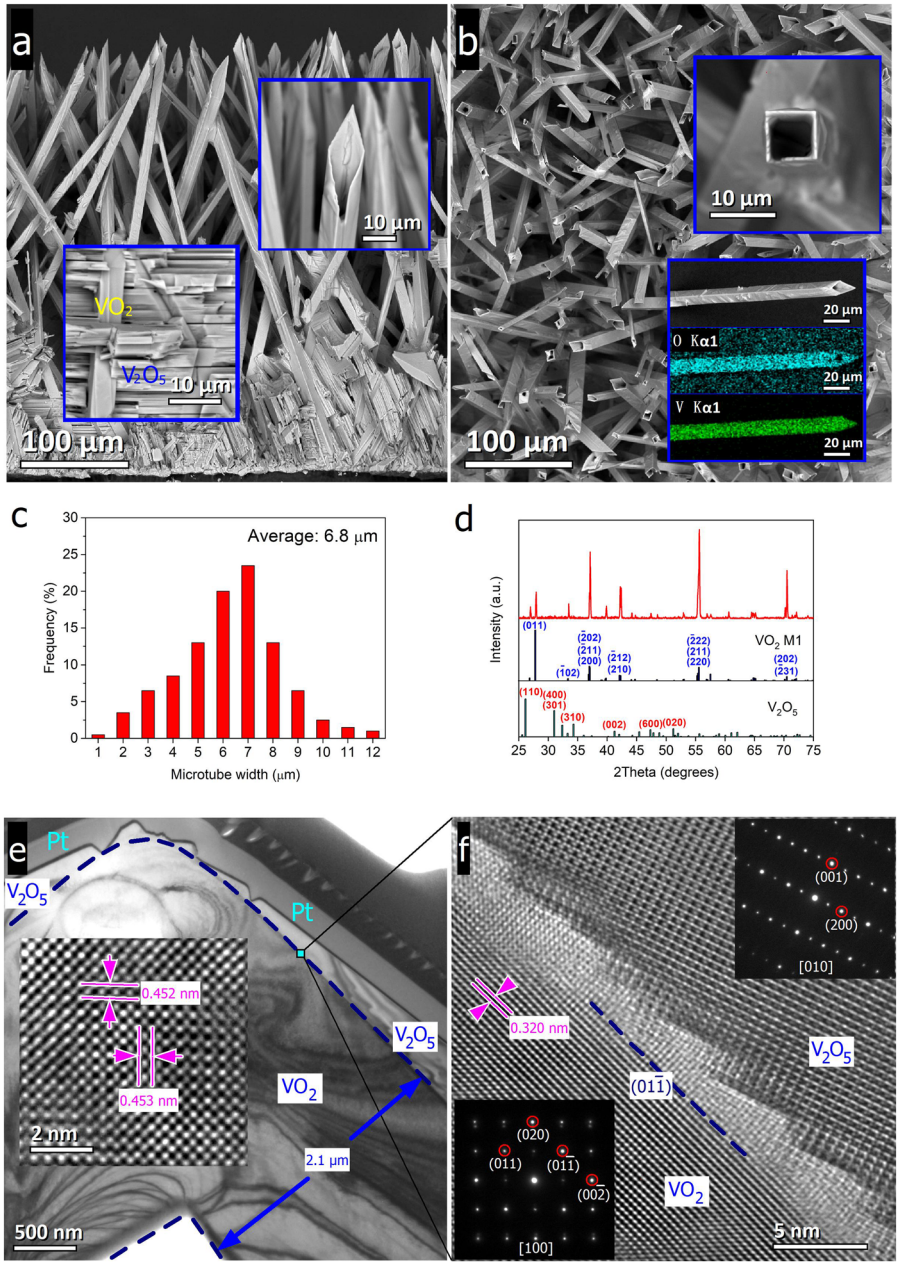

Fig. 2 Characteristics of single crystal VO_2 microtube arrays. a SEM image of the side view with the upper-right inset showing the top of a VO_2 microtube and the lower-left inset showing the bottom of a VO_2 microtube embedded in a layered V_2O_5 substrate. **b** SEM image of the top view with the upper-right inset showing the rectangular cross-section of a VO_2 microtube and the lower-right inset showing an individual VO_2 microtube with a uniform width and its EDS maps. **c** Histograms of the VO_2 microtube widths tabulated from the SEM images in (**a**) and (**b**). **d** XRD pattern at room temperature with standard powder diffraction patterns of the M1 phase of VO_2 and V_2O_5. **e** TEM image of a VO_2 microtube with the inset showing its HRTEM image. A Pt layer was added to protect the sample surface from contamination during TEM sample preparation. **f** HRTEM image of the boundary between the VO_2 and the V_2O_5 with the insets showing the electron diffraction images of the corresponding regions.

XPS spectra show a mixture of two vanadium oxidation states (i.e., V^{5+} and V^{4+}), which indicates that the vanadium in as-fabricated product features a mixed 4–5 oxidation state[33].

The crystal structure of the as-fabricated product was first examined using XRD at room temperature, and the diffraction pattern is shown in Fig. 2d. Clear and narrow diffraction peaks reveal that the as-fabricated product consists of high-quality crystals. The XRD peaks can be indexed unambiguously to the M1 phase of VO_2 (JCPDS card no. 72-0514) and orthorhombic phase of V_2O_5 (JCPDS card no. 41-1426), which confirms that the as-fabricated product only contains VO_2 and V_2O_5. Additional powder XRD pattern (Supplementary Fig. 6) also demonstrates that no other vanadium oxide can be identified except for VO_2 and V_2O_5. Moreover, very strong diffraction peaks that belong to the $\{2kl\}$ family of the M1 phase of VO_2 strongly suggest that the VO_2 microtube arrays have a preferred growth direction. Next, the microstructures of the VO_2 microtube and the V_2O_5 substrate were observed using TEM. Two cross-sectional TEM samples were prepared using focused ion beam (FIB) milling from different position of an individual microtube (Supplementary Fig. 7a, b). To avoid contamination of the sample surface by the FIB bombardment, a protective Pt layer was coated on the surface of the microtube during TEM sample preparation. Figure 2e depicts a TEM bright-field image of a corner of the microtube

with a VO_2 wall thickness of ~2.1 μm (the VO_2 is outlined with the navy dash lines). The corresponding HRTEM image (inset in Fig. 2e) displays the typical single crystal morphology of the M1 phase of VO_2 along the [100] zone axis (ZA), while the interplanar distance of 0.452 and 0.453 nm can be indexed as the (010) crystal plane and (001) crystal plane of the M1 phase of VO_2, respectively.

Furthermore, a thin layer of V_2O_5 with a thickness of less than 500 nm (marked in Fig. 2e) that is located on the side surface of the VO_2 microtube can be observed, which is the solidified V_2O_5 flux[25]. The microstructure of the solidified V_2O_5 flux and the crystallographic relation between the VO_2 and V_2O_5 were analyzed with an HRTEM image (Fig. 2f), which is a magnified image of the region in the cyan box located at the boundary between the VO_2 and V_2O_5 in Fig. 2e. The lower-left inset shows an electron diffraction image of single crystal VO_2 located in the lower-left region of Fig. 2f, which can be indexed to the [100] ZA of the M1 phase of VO_2. Thus, the side surface of the VO_2 microtube (marked with navy dashed lines in Fig. 2f) can be indexed to the $(01\bar{1})$ crystal plane with an interplanar distance of 0.320 nm, while another side surface of the VO_2 microtube shown in Fig. 2e can be indexed to the (011) crystal plane. The angle of these two crystal planes is 89.86°; thus, the VO_2 microtube appears to have a rectangular cross-section. The upper-right inset in Fig. 2f shows the corresponding electron diffraction image of the upper-right region in Fig. 2f, which can be indexed to the [010] ZA of V_2O_5. It is obvious that the boundary between the VO_2 and V_2O_5 is noncoherent. Electron diffraction pattern obtained from another TEM sample also demonstrates a single crystal VO_2 in $[100]_{M1}$ crystalline orientation (Supplementary Fig. 7c). Hence, TEM observations for two TEM samples clearly indicate that the microtube is single crystal VO_2 growing in $[100]_{M1}$ direction and confirm that the crystalline orientation remains the same across the entire VO_2 microtube. The growth direction of our single crystal VO_2 microtubes is the same as that of single crystal VO_2 fabricated by the vapor transport method[20,26], the self-flux method[22,23], and the hydrothermal method[27]. It is noted that the solidified V_2O_5 flux on the side surface of VO_2 microtubes can be easily removed (Supplementary Figs. 4a and 8b) by immersing the as-fabricated microtubes in a dilute aqueous solution of sodium carbonate with a concentration of 30 g/L for 30 min at room temperature based on the following reactions: $V_2O_5 + Na_2CO_3 \rightarrow 2NaVO_3 + CO_2\uparrow$[34].

Phase transition of single crystal VO_2 microtube arrays. The reversible MIT between the M1 and the R phases is the fundamental characteristic of VO_2. Thus, we carried out two differential scanning calorimetry (DSC) experiments for as-fabricated single crystal VO_2 microtube arrays. To analyze the thermal cycle stability, 28 heating and cooling cycles between 40 and 90 °C were carried out, and the DSC curves are depicted in Fig. 3a. These DSC curves show only one peak during each heating and cooling process, which indicates that as-fabricated single crystal VO_2 microtube arrays undergo a first-order phase transition. The phase transition peak temperatures of R → M1 (M_p) and M1 → R (R_p) for single crystal VO_2 microtube arrays are approximately 63.1 and 67.2 °C, respectively, which are in excellent agreement

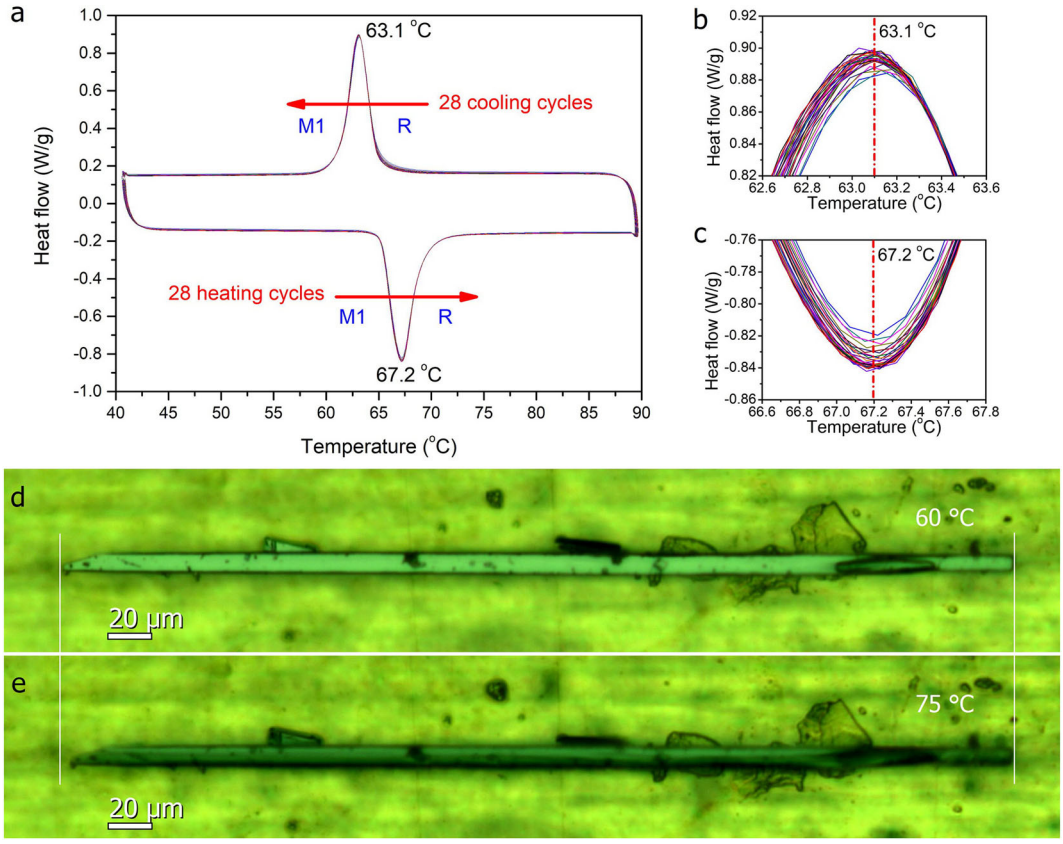

Fig. 3 Phase transition properties of single crystal VO_2 microtubes arrays. a DSC curves during 28 heating and cooling cycles, where 67.2 and 63.1 °C are the peak temperatures for the M1 → R and R → M1 phase transitions, respectively. **b** Magnified exothermal peaks and **c** magnified endothermal peaks of DSC curves that demonstrate the excellent thermal cycle stability of single crystal VO_2 microtube arrays. Optical images of an individual single crystal VO_2 microtube in **d** the M1 phase (60 °C) and **e** the R phase (75 °C) show not only a clear brightness change but also an obvious length shrinkage of ~0.7% along the $[100]_{M1}$ ($[001]_R$) axial direction across the phase transition from the M1 phase to the R phase as marked by the white lines.

with previously reported R_p of 67.8 °C for bulk single crystal VO_2[24], the R_p of 67.2 °C for single crystal VO_2 microrods[16], and the R_p of 67 °C for single crystal VO_2 nanowires[18]. This result indicates that our single crystal VO_2 microtube arrays have the same MIT property as single crystal VO_2 fabricated by the currently available methods. Most strikingly, the M_p and R_p of our VO_2 microtube arrays show almost no shift during 28 heating and cooling cycles, as shown in Fig. 3b, c. This finding confirms the excellent thermal cycle stability of the MIT process of our single crystal VO_2 microtube arrays. In contrast, VO_2 nanoparticles produced elsewhere were reported to have M_p and R_p shifts from 49.7 to 53.4 °C and from 61.0 to 68.8 °C, respectively, during seven heating and cooling cycles[35] because of the unstable microstructure of the VO_2 nanoparticles. Furthermore, it was reported that the M_p and R_p of a single crystal VO_2 microrod with a width of ~100 μm exhibited a run-to-run shift of up to ~1 °C during three heating and cooling cycles[16] because of the kinetic barrier of the first-order phase transition. In addition, a wide temperature range (−50 to 400 °C) DSC experiment was also carried out for exploring whether additional phase transitions can occur for the as-fabricated product, and the DSC curve is depicted in Supplementary Fig. 9. Same as Fig. 3a, the DSC curve shows only one peak during heating or cooling process, which indicates only MIT of M1 ↔ R can occur between −50 and 400 °C for single crystal VO_2 microtube arrays. Thus, the sharp peaks in the exothermal and endothermal scans of the DSC curve in Fig. 3a and Supplementary Fig. 9 indicate precise structural phase transitions, while the excellent exothermal and endothermal stabilities (Fig. 3b, c) suggest that our single crystal VO_2 microtube arrays have a very stable microstructure and great potential for device applications that require a long lifetime and a wide temperature range.

Moreover, we also carried out an optical microscope observation for an individual single crystal VO_2 microtube during a heating and cooling process and the optical images of the M1 phase at 60 °C and the R phase at 75 °C are shown in Fig. 3d, e (see also Supplementary Movie 2). Clear brightness change from bright to dark occurs uniformly for the whole microtube and corresponds to the insulator → metal transition, indicating a uniform stoichiometry and strain-free nature of single crystal VO_2 microtube[32]. And, an obvious length shrinkage of ~0.7% can be detected across the M1 → R phase transition due to the lattice constant differences along the $[100]_{M1}$ ($[001]_R$) axial direction; $a_{M1} = 0.5743$ nm (JCPDS card no. 72-0514) whereas $2c_R = 0.57028$ nm (JCPDS card no. 71-0565).

It is well known that the phase transition from the M1 phase to the R phase of VO_2 during heating corresponds to a colossal resistivity drop by over 4 orders of magnitude which can be reversible via a cooling process[11,12]. Thus, the phase transition of VO_2 can also be characterized by a resistance vs. temperature measurement, which can conclusively prove an MIT of VO_2. However, many factors such as electrical contact problem, metastable phases formation can bother the electrical data. In this work, the reversible MIT of single crystal VO_2 microtubes is revealed by the DSC and optical data. However, we do not present electrical data of single crystal VO_2 microtubes, which needs to be further studied in the future.

Discussion

Based on the experimental results, we propose a growth mechanism of single crystal VO_2 microtube arrays as illustrated in Fig. 4. According to the V–O phase diagram (inset in Supplementary Fig. 10)[30,31], VO_2 starts to crystallize just when the temperature of the liquid VO_x is lowered below the liquidous line. As shown in the cooling curve (Supplementary Fig. 10), the temperature of the liquid VO_x rapidly decreases from the peak temperature (1798 °C in Supplementary Fig. 10) to ~1542 °C (melting point of VO_2). The cooling curve starts to deviate the linear downtrend, which means VO_2 starts to nucleate in the liquid VO_x[36]. An additional SEM image of the side view of an as-fabricated product (Supplementary Fig. 11a) clearly shows that there is a layer of small equiaxed crystals with a thickness of ~12 μm at the bottom of the as-fabricated product. After immersion in a dilute aqueous solution of sodium carbonate for 10 min at room temperature, this layer of small equiaxed crystals does not have any change (Supplementary Fig. 11b), which is same as the status of the VO_2 microtubes. Hence, we propose that the VO_2 starts to nucleate at the V foil surface and then form a chill zone firstly, because the heat of the liquid VO_x dissipates much faster from the V foil than from the air after the heating is stopped. With continuous heat dissipation, some of these small equiaxed crystals then grow into the liquid VO_x and form arrays that are nearly vertically aligned on the surface of the V foil,

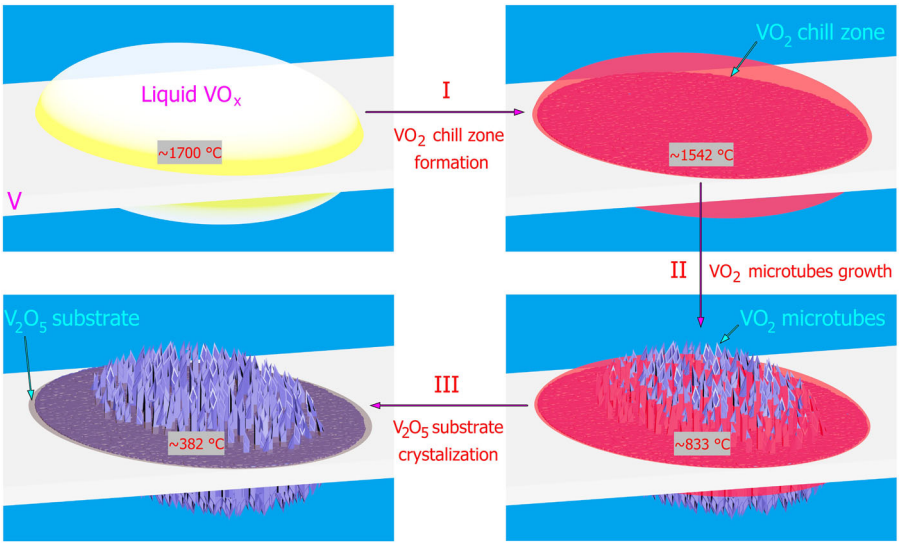

Fig. 4 Schematic illustrations of growth process of single crystal VO_2 microtube arrays. I VO_2 equiaxed crystals nucleate at the V foil surfaces and form the chill zones at ~1542 °C. **II** Single crystal VO_2 microtubes grow from the chill zones and form the arrays at ~833 °C. **III** Residual liquid VO_x crystallize and form the V_2O_5 substrate at ~382 °C.

because only those equiaxed crystals that are oriented favorably regarding the direction of heat flow can grow an appreciable distance and produce a columnar zone[37]. Thus, this process can be regarded as a directional growth, and the formation of the VO_2 microtube arrays is based on an interplay between the diffusion required for phase separation and the energy required for the formation of inter-phase boundaries[38]. TEM observations demonstrate that the VO_2 microtubes grow along the $[100]_{M1}([001]_R)$ direction and the bounding $(01\bar{1})_{M1}$ and $(011)_{M1}$ facets are crystallographically equivalent, low-index, and therefore, low energy surfaces[26]. The diameter and the spacing of the VO_2 microtubes are the result of a balance between two competing tendencies: on the one hand, to minimize the spacing in order to shorten the diffusion path of cations in the liquid VO_x, and on the other hand, to increase the spacing to minimize the total interfacial energy[38].

The formation of the hollow tubular structure of individual VO_2 microtube can be explained by the accumulation of top concave effect of rod-like crystals[39] as being similar to the growth mechanism of Se microtubes[40], W microtubes[41], SiAlON microtubes[42], and the wetting assisted growth mechanism of VO_x nanostructures[31]. The initial stage in the growth of a single crystal VO_2 microtube is the formation of a microparticle on the surface of the V foil followed by directional growth along the c-axis of R phase of VO_2 in the liquid droplet and then forming a rod-like VO_2 crystal as aforementioned scenario. In this anisotropic growth process, a mass transportation from the side surface to the top surface occurs, because the top surface grows much faster than the side surface of the rod-like VO_2 crystal[40–42]. Thus, the concentration of VO_2 at the edge of the top surface is higher than at the center, resulting growth rate at the edge is also higher than at the center[39]. Consequently, a concave shape produces at the top surface of the rod-like VO_2 crystal and the concavity of the top surface continuously increases by accumulation of the concave effect[42]. When the rod-like VO_2 crystal grows out of the liquid droplet, a thin liquid film wets the side surface of the rod-like VO_2 crystal along its entire length, creating a mass transportation channel for the rod-like VO_2 crystal growing top[31]. The growth continually takes place as feeding mass is transported to the growing top of the rod-like VO_2 crystal via the peripheral liquid wetting layer. However, for a fast growth process, mass transportation from the edge to the center of the growing top is very limited, which results in the growth stop of the center of the rod-like VO_2 crystal. As a consequence, a hollow tubular structure is eventually formed as shown in Fig. 2a, b.

When the temperature decreases to approximately 833 °C, the heat dissipation and the latent heat released by the crystallization of VO_2 reach an equilibrium, which results that temperature of the product is maintained at approximately 833 °C for a short time until the crystallization of VO_2 is complete. At this point, the residual liquidus composition of VO_x can be estimated by the equation: $x = -2.815 \times 10^{-4} T + 2.7015$[43], where T is the temperature in degrees centigrade. Here, the x is calculated to be 2.47 corresponding to the temperature of 833 °C, which is consistent with the EDS measurement result (Supplementary Fig. 4d). After the VO_2 crystallization finishes, the temperature of the residual liquid VO_x decreases again until to ~678 °C (melting point of V_2O_5). The cooling curve starts to deviate the linear downtrend again, which means V_2O_5 starts to nucleate in the residual liquid VO_x. This crystallization process lasts for a short time until the temperature reaches 382 °C, while the heat dissipation and the latent heat released by the crystallization of V_2O_5 reach an equilibrium. And the temperature can increase up to 409 °C as marked in Supplementary Fig. 10, because the latent heat released by the crystallization of V_2O_5 is greater than the heat dissipation during this process. It is noted that the obtained equilibrium temperature of 833 and 382 °C from cooling curve are much less than the melting point of VO_2 and V_2O_5, which we think it is because the crystallization process of the liquid VO_x is a nonequilibrium solidification. It is well known that the true crystallization temperature is actually very difficult to determine from a cooling curve because of the nonequilibrium conditions inherent in such a dynamic test for an actual solidification process[44].

Although single crystal VO_2 has demonstrated tremendous potential for practical use in various high-performance modern devices[11,12,18–21], critical issues remain unsolved and hinder the large-scale application of this smart material. Previous report shows that the phase transition of bulk single crystal VO_2 is very sharp and demonstrates relatively little hysteresis for heating and cooling rates of approximately 0.2 °C per minute[24]. Moreover, bulk single crystal VO_2 can be conveniently manipulated and assembled as a component in modern devices because its size is at the macroscale. However, microcracks that occur during heating and cooling because of the large (~1%) and anisotropic spontaneous strain associated with the MIT is a fatal drawback of bulk single crystal VO_2, which can result in degraded electronic and thermal properties[17]. Thus, the thermal cycle stability of bulk single crystal VO_2 is very poor, which makes it very unattractive for device applications[45]. It has been demonstrated that scaling VO_2 to the nanoscale can allow it to withstand an elevated uniaxial strain[46,47], thus enabling protracted thermal cycles without cracking during the MIT[48]. Hence, single crystal VO_2 nanowires are likely good candidates for device applications that require a long lifetime because they are free of extended structural defects during the MIT[17]. However, the existing techniques have not yet satisfied the requirements of large-scale applications of single crystal VO_2 nanowires[12], and additional engineering issues need to be solved, such as vertically aligning the nanowires on a substrate to form arrays for microbolometer sensing components[11], and improving the low yield due to the self-limiting in-plane growth[49]. In addition, it is difficult to use single crystal VO_2 nanowires for device applications because their scale is too small to be easily manipulated or assembled in an orderly fashion. Thus, convenient and high yield fabrication of vertical single crystal VO_2 arrays remains a challenging task.

Our single crystal VO_2 microtube arrays are likely able to solve these issues. The excellent thermal cycle stability demonstrates great potential for manufacturing devices with a long lifetime. Arrays that are nearly vertical should be very suitable for application such as microbolometer sensing components. Simple, fast, low-cost, and green fabrication processes are very convenient for high yield production. Moreover, our single crystal VO_2 microtube arrays are macroscopic and can be easily manipulated or assembled as a component in modern devices. Thus, we expect that single crystal VO_2 microtube arrays fabricated by our method can promote large-scale applications of VO_2 in various modern devices, such as microbolometers, lithium-ion batteries, supercapacitors, thermal emitters, and temperature sensors.

Methods

Fabrication. A commercially available pure V foil (99.9 wt%) with a thickness of 0.2 mm was used in this work. The V foil was cut into bars 3 mm wide and 20 mm long. In a typical procedure, a bar of V foil was mounted on two simple holders that was constructed in-house, which was connected to the positive and negative electrodes of a GW Instek PSB-2400L power supply with two wires (Supplementary Fig. 12a, b). Then, the V foil was resistively heated to approximately 1700 °C in tens of seconds by a direct current of <40 A in air. Afterwards, the direct current was turned off manually. The vanadium oxide product was formed in a few seconds on the central surface of both sides of V foil (marked by an arrow in Supplementary Fig. 12c). The slow heating/cooling rate was controlled by manual adjusting the rotary knob of the power supply which changed the applied direct current. Whereas, the rapid cooling rate was realized by turning off the direct current at the peak temperature of each fabrication run. Supplementary Fig. 12d shows an SEM image of an as-fabricated product. The single crystal VO_2 microtube arrays are

mainly located in the central region of the product, while the substrate is a layered V_2O_5. The fabrication temperature was monitored by a pyrometer (LumaSense IGAR 6 Advanced with a temperature range of 250–2000 °C, a resolution of 0.1 °C, and a sampling rate of 60 s^{-1}). Ambient conditions corresponded to regular laboratory and atmospheric pressure condition with a temperature range of 15–35 °C, a relative humidity range of 11–100%, and an oxygen partial pressure of ~21.2 kPa.

Morphology observation and composition determination. The morphology of the as-fabricated product was mainly observed using a Hitachi TM3030 scanning electron microscope equipped with an Oxford Swift 3000 X-ray energy dispersive spectroscope for element mapping. Moreover, an as-fabricated product was immersed in a dilute aqueous solution of sodium carbonate for 30 min at room temperature, followed by EDS analysis using a Hitachi SU8220 scanning electron microscope equipped with an Oxford X-Max X-ray energy dispersive spectroscope. The X-ray photoelectron spectroscopy was obtained using a Thermo Scientific ESCALAB 250Xi X-ray photoelectron spectrometer.

Structure characterizations. XRD examination was carried out using a Rigaku SmartLab X-ray diffractometer at room temperature. An as-fabricated product directly underwent XRD examination by putting the whole product on a plain sample stage without any treatment. Then, three as-fabricated products were ground into powder by an agate mortar, followed by XRD examination again. Two cross-sectional TEM samples from an individual microtube were prepared using a Helios NanoLab 600 focused ion beam scanning electron microscope. A TEM sample of V_2O_5 substrate was prepared by conventional method for powder samples. The TEM samples were observed using a FEI Tecnai G2 F20 S-TWIN transmission electron microscope at 200 kV.

Phase transition analysis. The DSC experiments were carried out using a TA Q2000 calorimeter. Three as-fabricated products (15.4 mg in all) were directly put into a Tzero pan for a 28 thermal cycles DSC experiment. The temperature range was 40–90 °C, and the heating and cooling rates were 10 °C/min. Other three as-fabricated products (14.3 mg in all) were also directly put into a Tzero pan for a wide temperature range DSC experiment. The temperature range was −50 to 400 °C, and the heating and cooling rates were 10 °C/min also. Optical microscope observation was carried out using a Leica DMLM microsystem with a heating stage.

Data availability

The data that support the findings of this study are available from the corresponding author upon reasonable request.

Received: 7 December 2019; Accepted: 25 April 2020;
Published online: 15 May 2020

References

1. Valle, J. et al. Subthreshold firing in Mott nanodevices. *Nature* **569**, 388–392 (2019).
2. Otto, M. R. et al. How optical excitation controls the structure and properties of vanadium dioxide. *Proc. Natl. Acad. Sci. U.S.A.* **116**, 450–455 (2019).
3. Lee, D. et al. Isostructural metal-insulator transition in VO_2. *Science* **362**, 1037–1040 (2018).
4. Vaseem, M., Zhen, S., Yang, S., Li, W. & Shamim, A. development of VO_2-nanoparticle-based metal-insulator transition electronic ink. *Adv. Electron. Mater.* **5**, 1800949 (2019).
5. Liu, B. T. et al. Extraordinary pseudocapacitive energy storage triggered by phase transformation in hierarchical vanadium oxides. *Nat. Commun.* **9**, 1375 (2018).
6. Fiorino, A. et al. A thermal diode based on nanoscale thermal radiation. *ACS Nano* **12**, 5774–5779 (2018).
7. Sun, R. et al. Broadband switching of mid-infrared atmospheric windows by VO_2-based thermal emitter. *Opt. Express* **27**, 11537−11546 (2019).
8. Chen, S. et al. Gate-controlled VO_2 phase transition for high-performance smart windows. *Sci. Adv.* **5**, eaav6815 (2019).
9. Baqir, M. A. & Choudhury, P. K. On the VO_2 metasurface-based temperature sensor. *J. Opt. Soc. Am. B* **36**, F123−F130 (2019).
10. Ordonez-Miranda, J., Ezzahri, Y., Tiburcio-Moreno, J. A., Joulain, K. & Drevillon, J. Radiative thermal memristor. *Phys. Rev. Lett.* **123**, 025901 (2019).
11. Liu, K., Lee, S., Yang, S., Delaire, O. & Wu, J. Recent progresses on physics and applications of vanadium dioxide. *Mater. Today* **21**, 875–896 (2018).
12. Shi, R. et al. Recent advances in fabrication strategies, phase transition modulation, and advanced applications of vanadium dioxide. *Appl. Phys. Rev.* **6**, 011312 (2019).
13. Graf, D., Schläfer, J., Garbe, S., Klein, A. & Mathur, S. Interdependence of structure, morphology, and phase transitions in CVD grown VO_2 and V_2O_3 nanostructures. *Chem. Mater.* **29**, 5877–5885 (2017).
14. Kim, H. J., Roh, D. K., Jung, H. S. & Kim, D. S. Size and shape control of monoclinic vanadium dioxide thermochromic particles for smart window applications. *Ceram. Int.* **45**, 4123–4127 (2019).
15. Hu, F. et al. Electrically triggered tunable terahertz band-pass filter based on VO_2 hybrid metamaterial. *IEEE J. Sel. Top. Quantum Electron.* **25**, 4700207 (2019).
16. Mun, B. S. et al. Nonpercolative metal-insulator transition in VO_2 single crystals. *Phys. Rev. B* **84**, 113109 (2011).
17. Lee, S. et al. Anomalously low electronic thermal conductivity in metallic vanadium dioxide. *Science* **355**, 371–374 (2017).
18. Lee, S. et al. Axially engineered metal–insulator phase transition by graded doping VO_2 nanowires. *J. Am. Chem. Soc.* **135**, 4850–4855 (2013).
19. Liu, Q. et al. Revealing mechanism responsible for structural reversibility of single crystal VO_2 nanorods upon lithiation/delithiation. *Nano Energy* **36**, 197–205 (2017).
20. Shi, R. et al. Single-crystalline vanadium dioxide actuators. *Adv. Funct. Mater.* **29**, 1900527 (2019).
21. Lee, H. J. et al. Directional Ostwald ripening for producing aligned arrays of nanowires. *Nano Lett.* **19**, 4306–4313 (2019).
22. Yoon, J. et al. Controlling the temperature and speed of the phase transition of VO_2 microcrystals. *ACS Appl. Mater. Interfaces* **8**, 2280–2286 (2016).
23. Sasaki, H. & Watanabe, A. New growing method for VO_2 single crystals. *J. Phys. Soc. Jpn.* **19**, 1748 (1964).
24. Liu, M. et al. Phase transition in bulk single crystals and thin films of VO_2 by nanoscale infrared spectroscopy and imaging. *Phys. Rev. B* **91**, 245155 (2015).
25. Kong, T., Masters, M. W., Budko, S. L. & Canfield, P. C. Physical properties of $V_{1-x}Ti_xO_2$ ($0 < x < 0.187$) single crystals. *APL Mater.* **3**, 041502 (2015).
26. Guiton, B. S., Gu, Q., Prieto, A. L., Gudiksen, M. S. & Park, H. Single-crystalline vanadium dioxide nanowires with rectangular cross sections. *J. Am. Chem. Soc.* **127**, 498–499 (2005).
27. Shi, R. et al. Axial modulation of metal–insulator phase transition of VO_2 nanowires by graded doping engineering for optically readable thermometers. *J. Phys. Chem. C* **121**, 24877–24885 (2017).
28. Jiang, X., Herricks, T. & Xia, Y. CuO nanowires can be synthesized by heating copper substrates in air. *Nano Lett.* **2**, 1333–1338 (2002).
29. Rackauskas, S. et al. A novel method for metal oxide nanowire synthesis. *Nanotechnology* **20**, 165603 (2009).
30. Wriedt, H. A. The O–V (oxygen–vanadium) system. *Bull. Alloy Phase Diagr.* **10**, 271–277 (1989).
31. Strelcov, E., Davydov, A. V., Lanke, U., Watts, C. & Kolmakov, A. In situ monitoring of the growth, intermediate phase transformations and templating of single crystal VO_2 nanowires and nanoplatelets. *ACS Nano* **5**, 3373–3384 (2011).
32. Cheng, C., Liu, K., Xiang, B., Suh, J. & Wu, J. Ultra-long, free-standing, single-crystalline vanadium dioxide micro/nanowires grown by simple thermal evaporation. *Appl. Phys. Lett.* **100**, 103111 (2012).
33. Silversmit, G., Depla, D., Poelman, H., Marin, G. B. & Gryse, R. D. Determination of the V2p XPS binding energies for different vanadium oxidation states (V^{5+} to V^{0+}). *J. Electron Spectrosc. Relat. Phenom.* **135**, 167–175 (2004).
34. Li, X., Xie, B. & Ran, J. Extraction of vanadium pentoxide from low grade vanadium slag with high silicon and high calcium. *Chin. J. Rare Metals* **35**, 747–752 (2011).
35. Li, M. et al. In situ triggering and dynamically tracking the phase transition in vanadium dioxide. *J. Phys. Chem. C* **118**, 16279–16283 (2014).
36. Fukuyama, H., Sawada, R., Nakashima, H., Ohtsuka, M. & Yoshimi, K. Study of solidification pathway of a MoSiBTiC alloy by optical thermal analysis and in-situ observation with electromagnetic levitation. *Sci. Rep.* **9**, 15049 (2019).
37. Bramfitt, B. L. Solidification structures of steel. In *Metallography and Microstructures. ASM Handbook*, **Vol. 9** (ASM International, 1992).
38. Hassel, A. W., Bello-Rodriguez, B., Smith, A. J., Chen, Y. & Milenkovic, S. Preparation and specific properties of single crystalline metallic nanowires. *Phys. Status Solidi B* **247**, 2380–2392 (2010).
39. Kitayama, M., Hirao, K., Toriyama, M. & Kanzaki, S. Modeling and simulation of grain growth in Si_3N_4. III. Tip shape evolution. *Acta Mater.* **48**, 4635–4640 (2000).
40. Filippo, E., Manno, D. & Serra, A. Aligned selenium microtubes array: synthesis, growth mechanism and photoelectrical properties. *Chem. Phys. Lett.* **510**, 87–92 (2011).
41. Wang, S. et al. Large-scale synthesis of tungsten single-crystal microtubes via vapor-deposition process. *J. Cryst. Growth* **316**, 137–144 (2011).
42. Liu, G., Chen, K. & Li, J. Growth mechanism of crystalline SiAlON microtubes prepared by combustion synthesis. *CrystEngComm* **14**, 5585–5588 (2012).
43. Suito, H. & Gaskell, D. R. The thermodynamics of melts in the system VO_2–V_2O_5. *Metall. Trans.* **2**, 3299–3303 (1971).

44. Baker, H. Introduction to alloy phase diagrams. In *Alloy Phase Diagrams. ASM Handbook*, **Vol. 3** (ASM International, 1992).
45. Budai, J. D. et al. In situ X-ray microdiffraction studies inside individual VO_2 microcrystals. *Acta Mater.* **61**, 2751–2762 (2013).
46. Cao, J. et al. Strain engineering and one-dimensional organization of metal–insulator domains in single-crystal vanadium dioxide beams. *Nat. Nanotechnol.* **4**, 732–737 (2009).
47. Hu, B. et al. External-strain induced insulating phase transition in VO_2 nanobeam and its application as flexible strain sensor. *Adv. Mater.* **22**, 5134–5139 (2010).
48. Horrocks, G. A., Singh, S., Likely, M. F., Sambandamurthy, G. & Banerjee, S. Scalable hydrothermal synthesis of free-standing VO_2 nanowires in the M1 phase. *ACS Appl. Mater. Interfaces* **6**, 15726–15732 (2014).
49. Cheng, C. et al. Self-assembly and horizontal orientation growth of VO_2 nanowires. *Sci. Rep.* **4**, 5456 (2014).

Acknowledgements

This work was supported by the National Natural Science Foundation of China (Nos. 11972221 and 11672175). The authors acknowledge Dr. G.R. Xu (IMUT) and Prof. Z.Z. Cao (IMUT) for the help of XRD examination, Dr. X.H. Hou (IMUT) for the help of EDS testing, and Dr. F.C. Lang (IMUT) and Y.J. Jin (IMUT) for the help of optical measurement.

Author contributions

C.Z. and Y.X. conceived and designed the experiments. S.M. and Z.L. carried out the fabrication of materials and the microstructural characterizations. W.L. performed the DSC experiment. C.Z., J.L., Q.H., and Y.X. analyzed the experimental results and wrote the manuscript. All authors commented on the manuscript.

Competing interests

The authors declare no competing interests.

Additional information

Supplementary information is available for this paper at https://doi.org/10.1038/s43246-020-0031-4.

Correspondence and requests for materials should be addressed to C.Z. or Y.X.

Reprints and permission information is available at http://www.nature.com/reprints

Publisher's note Springer Nature remains neutral with regard to jurisdictional claims in published maps and institutional affiliations.